

Computational mechanics of multiphase materials – modeling strategies at different scales

Günther Meschke, Dirk Leonhart,
Jithender J. Timothy, Meng-Meng Zhou
Institute for Structural Mechanics
Ruhr University Bochum
44780 Bochum, Germany
e-mail: guenther.meschke@rub.de

The paper addresses various scale-bridging modeling and discretization strategies for multiphase porous materials, starting with a micromechanics model for ion transport within the pore space to generate homogenized diffusion coefficients. Using homogenized macroscopic properties, the theory of poromechanics provides the modeling framework for the macroscopic representation of transport and phase change processes as it is demonstrated for freezing of porous materials using a three-field formulation. The theory of poromechanics is again employed as an appropriate representation of more or less intact porous materials, in conjunction with a two-field Extended Finite Element model as a scale bridging tool to describe coupled hydro-mechanical processes in cracked porous materials at a macroscopic level.

Keywords: micromechanics, poromechanics, Extended Finite Element Method, homogenization, multi-phase models, diffusion, durability, soil freezing.

1. INTRODUCTION

Computational simulations of structures made of heterogeneous porous materials such as concrete or soil, when subjected to combined mechanical, thermal, hygral or chemical loading, require an adequate representation of the multiphase character of the problem, considering the highly interacting multi-physics (mechanical, hygric, thermal and chemical) processes acting within the microstructure. These processes are closely related to the changing pore structure of the material and to micro-defects eventually evolving to macro-cracks. Since, for structural simulations, the model description eventually is formulated on a macroscopic level, methods of scale transition must be applied in conjunction with adequate discretization strategies for the solution of the governing equilibrium and balance equations. In the framework of a true multiscale approach, assuming that the principle of scale separation holds [40], the individual scales are described as a series of nested boundary value problems, using appropriate (e.g., periodic) boundary conditions (see, e.g., [17, 26]). In such multiscale finite element models (often denoted as FE²-models, if two scales are considered), the constituents are described by means of classical continuum mechanics models for one-phase materials, formulating appropriately the interactions between the constituents and the contact conditions, respectively. To this end, the exact knowledge of the morphology of the material, in particular of the geometry of the pore space, is required. This is, however, not available in general. This difficulty motivates the description of porous materials on the basis of an a priori macroscopic approach. With regards to up-scaling methods, three modeling frameworks suitable for the homogenization of microscopic or submicroscopic quantities are discussed in the paper: the Theory of Porous Media as a classical averaging method and methods of micromechanics for the up-scaling of transport properties within the highly tortuous pore structure, ranging from

the nanometer to the micrometer scale, and the state of (distributed) damage and the variational multiscale method bridging scales on the level of the finite element approximations. As far as the second aspect is concerned, the finite element method for the analysis of intact materials as well as the Extended Finite Element Method (XFEM) [27] for the analysis of cracked multiphase materials will be addressed.

The paper is organized within three parts. The first part will be concerned with the determination of up-scaled transport properties for ion diffusion in cementitious materials, both for the damaged as well as for a state characterized by a more or less diffuse distribution of microcracks. Homogenized material properties such as diffusion coefficients or liquid permeabilities can be directly used in durability models for multiphase solids using more classical up-scaling concepts such as the theory of poromechanics. This theory is used as the framework for a three-phase model for frozen soils in the second part of the paper. In the third part, the incorporation of cracks – constituting disturbances at a small scale compared to the larger uncracked part – is accomplished using the Extended Finite Element Method (XFEM) as a variational multiscale type approach [16] in the context of two-field hygro-mechanical problems.

2. DIFFUSION IN INTACT AND MICRO-CRACKED POROUS MATERIALS: UP-SCALING FROM NANO- TO MACROSCALE USING CONTINUUM MICROMECHANICS

In modeling molecular transport in porous materials using the diffusion equation on the macroscopic level, the prerequisite for adopting a homogenized material property relevant for ion transport, denoted as the diffusion coefficient, is, that it captures the underlying heterogeneity of the microstructure in terms of certain microstructure characterizing variables. In heterogeneous porous materials, such as concrete or geological materials, the microstructure is highly tortuous and covers various scales. Table 1 contains a classification of the pore space of concrete [18, 34]. In phenomenological approaches, the microstructure of porous material effects are captured by the volume fraction of the pore-space and the so-called tortuosity factor [32]. The tortuosity factor used to account for the pore connectivity, constrictivity and pore space topology was obtained experimentally, constructed empirically or from pore network models. Recently continuum micromechanics [11] was employed to establish a mathematical model for the tortuosity factor. An alternative approach based on the Minkowski metric space to characterize an anisotropic pore space is presented in [5]. The tortuosity is defined as the ratio of the lengths in the Minkowski space and Euclidean space respectively.

Table 1. Classification of concrete porosity [34].

Type of pore	Hydr. radius	Characteristics	Type of pore water
Coarse	≥ 1 mm	empty	
Macro-capillary	< 1 mm	sucking, immediately refillable	free macroscopic water, freezable, highly mobile, small capillary rise.
Meso-capillary	< 30 μ m	sucking within minutes, refillable within weeks	free macroscopic water, freezable, considerable capillary rise within a few days
Micro-capillary	< 1 μ m	no stationary state	macroscopic water, freezable, strong capillary attraction, but increasing internal friction
Meso-gel	< 30 nm	Transition from the free, macroscopic behaviour to surface physics; filled by condensation at 50% to 98% relative humidity	pre-structured, condensed water, evaporation below 50% relative humidity, not freezable beyond -23° C
Micro-gel	< 1 nm	surface physics, filled by sorption below $< 50\%$ relative humidity	structured surface water, strongly disturbed, not freezable

2.1. Ion diffusion in the pore space

At the lowest level of description, molecular transport in concentrated ionic pore solutions must be described mathematically. An adequate electrolyte model for concentrated pore solutions is given by the ONSAGER-FUOSS diffusion model, which provides a diffusion coefficient as [29]

$$D^{OF} = [D_0 + \Delta] \left[1 + c \frac{d \ln \gamma_{\pm}}{dc} \right]. \quad (1)$$

D_0 is the diffusion coefficient for the infinitely diluted case. $c \frac{d \ln \gamma_{\pm}}{dc}$ corresponds to the relaxation effect due to the interaction of the electrostatic forces and the BROWNIAN motion and Δ is the electrophoretic effect due to the viscosity induced mobility imbalance of the ions.

A five parameter concentration dependent diffusion coefficient of electrolyte solutions, which is a synthesis of the ONSAGER-FUOSS diffusion model by approximating the molar activity coefficient using the DEBYE-HÜCKEL theory, has been proposed in [21]:

$$D^{OF} = D_0 + \frac{A_1 \kappa}{1 + \kappa a} + \frac{D_0 A_3 \kappa}{(1 + \kappa a)^2} + \frac{A_1 A_3 \kappa^2}{(1 + \kappa a)^3}. \quad (2)$$

2.2. Up-scaling framework

For up-scaling of the transport coefficients we initially consider a two-scale problem and establish a set of relations between the scales. This framework can be applied in a straightforward manner for multiple scales, provided that the REV in question exists. A point at the macroscopic scale, described by the position vector, represents a Representative Elementary Volume (REV) with a certain micro-structure at the microscopic scale, characterized by a local reference frame with spatial positions defined in terms of the variable \mathbf{z} . With regard to molecular transport, the driving force for diffusion is the concentration gradient vector field ∇c . Assuming macroscopic homogeneity, the force balance between the scales is obtained by averaging the concentration gradients at the microscopic scale,

$$\frac{1}{\Omega_{\text{REV}}} \int_{\Omega_{\text{REV}}} (\nabla_{\mathbf{z}} c(\mathbf{z})) d\Omega_{\text{REV}} = \nabla_{\mathbf{x}} c(\mathbf{x}). \quad (3)$$

We introduce a function $\mathcal{A}(\mathbf{z})$ defined on the microscopic scale, whose up-scaling from the microscopic scale gives the identity tensor:

$$\frac{1}{\Omega_{\text{REV}}} \int_{\Omega_{\text{REV}}} (\mathcal{A}(\mathbf{z})) d\Omega_{\text{REV}} = \mathbf{I}. \quad (4)$$

From Eq. (3) and Eq. (4), for an arbitrary REV follows,

$$\nabla_{\mathbf{z}} c(\mathbf{z}) = \mathcal{A}(\mathbf{z}) \cdot \nabla_{\mathbf{x}} c(\mathbf{x}). \quad (5)$$

$\mathcal{A}(\mathbf{z})$ represents a localization tensor as the local concentration gradient in the REV, obtained by post multiplication of the macroscopic concentration gradient, which, as a consequence of macroscopic homogeneity, is not a function of \mathbf{x} . It can be inferred that the localization tensor has complete information regarding the micro-structure.

The diffusion equation is constructed at the microscopic scale. It must be noted that the diffusion coefficient $D(\mathbf{z})$ at the scale of the micro-structure is position dependent. The link to the macroscopic scale is accomplished at the boundary Γ_{REV} , where the concentration c is obtained

from the macroscopic concentration gradient. The steady state boundary value problem can thus be summarized as follows:

$$c(\mathbf{z}) = \nabla_{\mathbf{x}} c \cdot \mathbf{z}, \quad \forall \mathbf{z} \in \Gamma_{\text{REV}}, \quad (6)$$

$$\nabla_{\mathbf{z}} \cdot \mathbf{j}(\mathbf{z}) = 0, \quad \forall \mathbf{z} \in \Omega_{\text{REV}},$$

$$\mathbf{j}(\mathbf{z}) = -D(\mathbf{z}) \cdot \nabla_{\mathbf{z}} c(\mathbf{z}), \quad \forall \mathbf{z} \in \Omega_{\text{REV}}. \quad (7)$$

The macroscopic flux is given by

$$\frac{1}{\Omega_{\text{REV}}} \int_{\Omega_{\text{REV}}} (\mathbf{j}(\mathbf{z})) d\Omega_{\text{REV}} = \mathbf{J}. \quad (8)$$

We now consider a multiphase material with N phases. Using the localization tensor \mathcal{A}_i , the macroscopic ion flux is given by the averaged diffusion coefficient D_i in phase i

$$\mathbf{J} = -\frac{1}{\Omega_{\text{REV}}} \left(\sum_{i=1}^N D_i \mathcal{A}_i \int_{\Omega_{\text{REV}}^i} d\Omega_{\text{REV}}^i \right) \nabla_{\mathbf{x}} c(\mathbf{x}). \quad (9)$$

\mathcal{A}_i is computed by solving the ESHELBY [12] matrix inclusion problem using the ESHELBY tensor.

2.3. Up-scaled diffusion coefficients for cracked and un-cracked porous materials

The localization tensor is computed using the ESHELBY method for a spherical pore characterizing the isotropic distribution of pore channels with arbitrary diameters in a non-solid porous matrix characterized by a diffusion coefficient $D^h = D^{OF} \phi$, where ϕ is the porosity, see Fig. 1. For porous materials it can be inferred from Eq. (9) that the inverse of the phase specific localization tensor is the phenomenological tortuosity parameter. A value of 1 for the localization tensor would mean that the pore geometry has no effect on transport and the only quantity that affects transport is the pore volume fraction. This geometrical character of the tortuosity is also suggested in [5]. The localization tensor for a spherical inclusion in a matrix with the diffusion coefficient $D^h = D^{OF} \phi$ is obtained as,

$$\mathcal{A}_f^1 = \frac{3D^h}{2D^h + D^{OF}} \mathbf{I}. \quad (10)$$

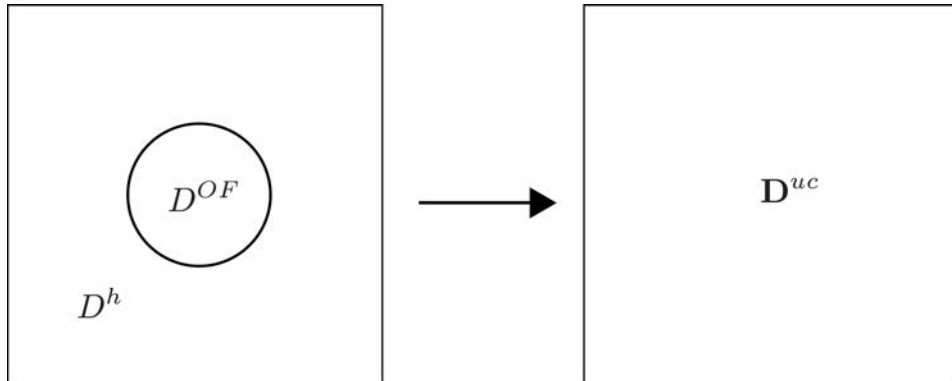


Fig. 1. Diffusion coefficients in intact (un-cracked) porous materials obtained from the continuum micromechanics model.

Using Eq. (9), the homogenized diffusion coefficient for un-cracked porous materials idealized as a two phase material with the diffusion coefficient in the solid phase as zero follows [35, 36]:

$$\mathbf{D}^{uc} = D^{OF} \mathcal{A}_f^n \phi. \quad (11)$$

Using a similar scheme as employed in homogenizing the intact porous material; however, considering now micro-cracks modeled as oriented ellipsoidal inclusions (see Fig. 3), we obtain, for penny shaped ellipsoids, micro-cracks embedded within an intact porous matrix as sketched in Fig. 2,

$$\frac{\mathbf{D}^c}{D^{OF}} = \varphi_c \mathbf{\Upsilon} + \frac{\mathbf{D}^{uc}}{D^{OF}}. \quad (12)$$

φ_c denotes the crack-volume fraction (which plays a similar role as a damage variable in damage mechanics) and $\mathbf{\Upsilon}$ is an interaction tensor that considers the effect of the surrounding pores on the micro-cracks and the orientation and topology (see [37] for details).

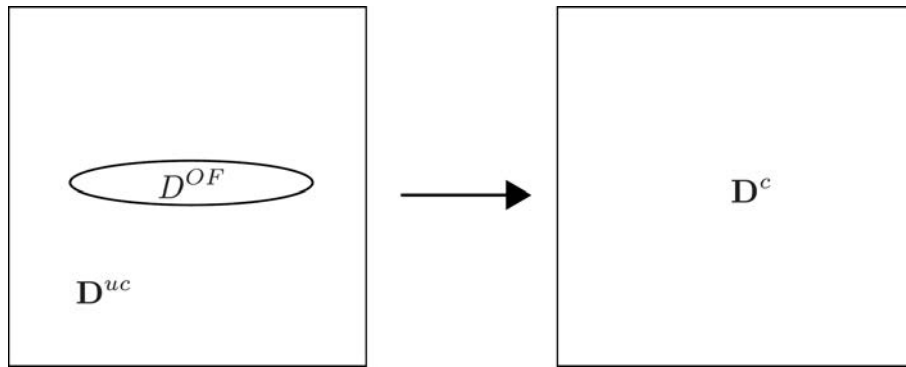


Fig. 2. Diffusion coefficient in cracked porous materials obtained from the continuum micromechanics model.

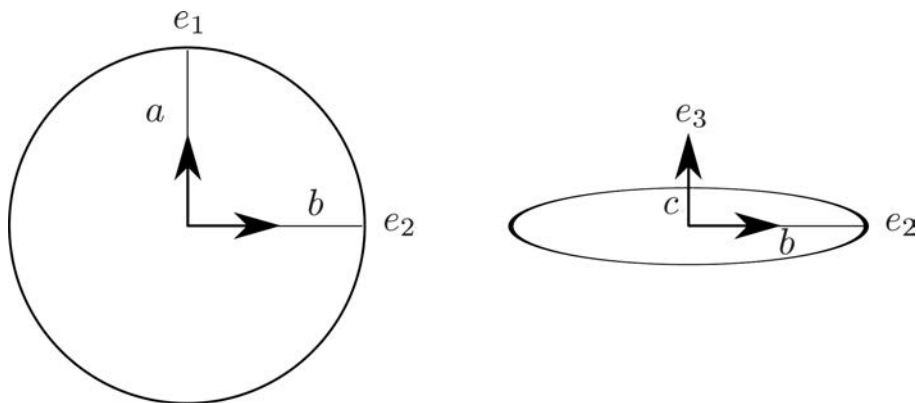


Fig. 3. Micro-crack geometry idealized as a penny shaped ellipsoid.

The effect of the aspect ratio of the micro-crack is given in Fig. 4. The results are plotted for the normalized diffusion coefficient against the pore volume fraction and the micro-crack volume fraction parallel to the plane perpendicular to the unit vector \mathbf{e}_3 (see Fig. 3). It is observed, for constant pore volume fraction, that as the aspect ratio decreases the flux increases. From this observation it can be inferred that micro-cracks highly affect the transport properties of porous materials by providing an increased connectivity of the porous matrix in the direction of the orientation of the micro-cracks.

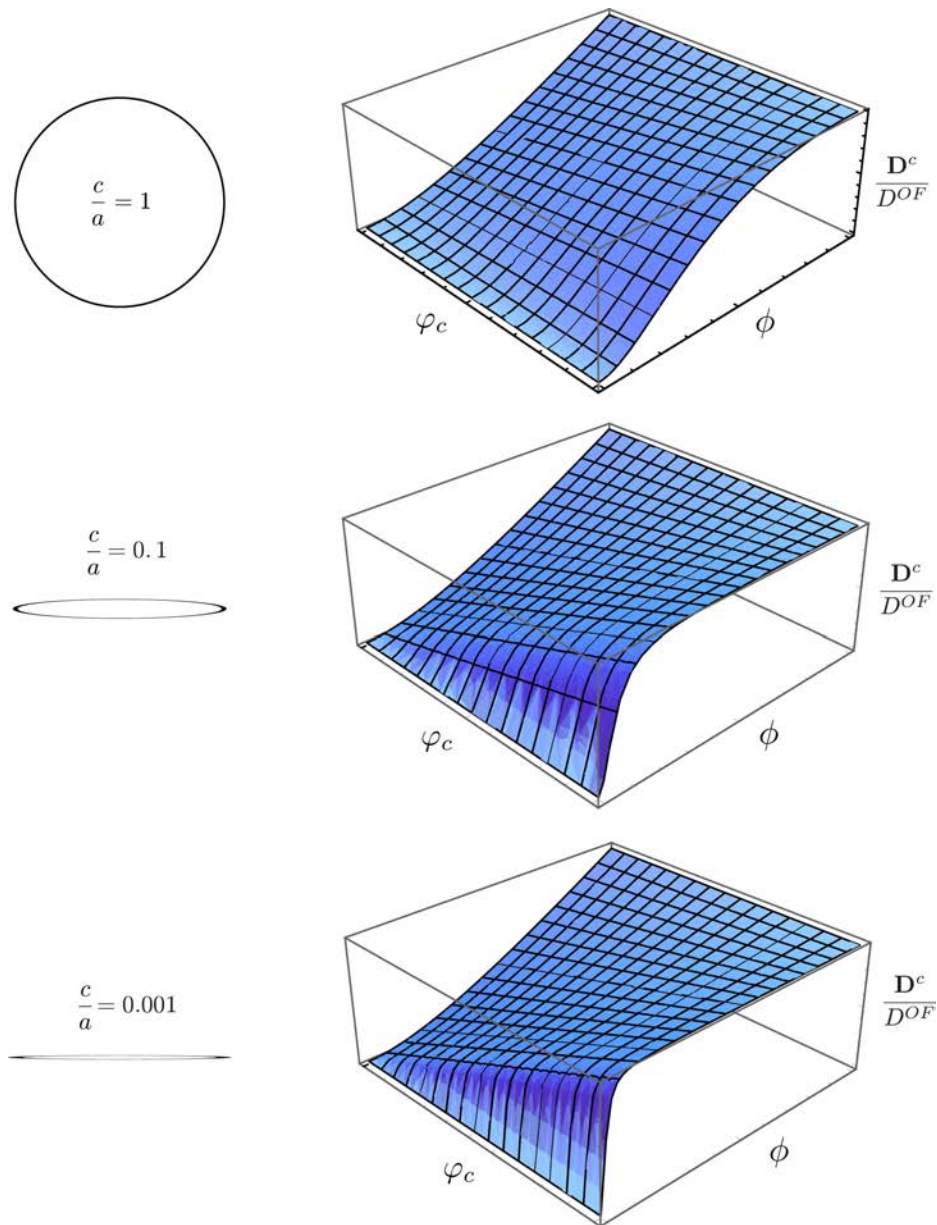


Fig. 4. Effect of the aspect-ratio $\left(\frac{c}{a}\right)$ of distributed micro-cracks on the homogenized diffusion coefficient in the plane perpendicular to \mathbf{e}_3 . $\left(0 \leq \left(\phi, \varphi_c, \frac{\mathbf{D}^c}{D^{OF}}\right) \leq 1\right)$.

2.4. Application to chemo-mechanical damage of concrete

Chemically aggressive substances in contact with the cementitious matrix of concrete may lead to the de-calcification of the cement matrix, and, consequently, to the long term degradation of the material. Since the micro-structure and the chemical composition of the cementitious matrix change, the macroscopic mechanical and transport properties of concrete change. The degree of dissolution depends on chemical conditions of the fluid as well as on environmental conditions. Cooling towers, containments for nuclear or other waste disposal, cement-bound coatings of drinking water reservoirs, grouted anchors and tunnel linings are examples of structures and structural components, respectively, potentially exposed to aggressive environments connected with dissolution processes [34]. Based on BERNER's experimental data, a chemical equilibrium model, characterized by a relation $s(c)$ between the calcium concentration in the pore fluid c and the calcium concentration

of the cementitious skeleton s has been proposed by [10, 13], assuming instantaneous dissolution processes, i.e. neglecting the kinetics of the chemical process. This phenomenological chemical equilibrium model, together with the electrolyte diffusion model 2 was taken as the starting point for a chemo-mechanical damage model proposed in [19].

The porosity ϕ can be defined as the sum of the initial porosity related to the virgin material ϕ_0 and the chemical porosity ϕ_{chem} resulting from the skeleton dissolution. The actual void-fraction contribution associated with the opening of micro-cracks is φ_c^a . The crack volume fraction as defined in the proposed multi-scale micromechanics model is defined for $0 \leq \varphi_c \leq 1$. Thus, it can be directly used as the variable characterizing damage and no new damage variable needs to be defined. However, φ_c is not the actual volume fraction of micro-cracks. The total void fraction associated with the pore-space and micro-cracks is

$$\phi_T = \phi + \varphi_c^a = \phi_0 + \phi_{chem} + \varphi_c^a. \quad (13)$$

The actual volume fraction of the cracks can be obtained from the following relation:

$$\varphi_c^a = \varphi_c - \varphi_c \phi. \quad (14)$$

Equation (14) is obtained by equating $\phi_T = \phi + \varphi_c^a$ and the alternate definition used in the proposed multiscale model $\phi_T = \varphi_c + (1 - \varphi_c)\phi$ and solving for the actual crack volume fraction.

The coupled mechanism of calcium leaching and mechanical damage of cementitious materials is governed by the macroscopic mass balance of calcium ions dissolved within the aqueous pore fluid and by the balance equation of momentum. The mass balances are described in terms of the concentration of calcium ions Ca^{++} within the pore fluid c , the molar calcium ion production from dissociation \dot{s} , the total void fraction ϕ_T and the stress tensor $\boldsymbol{\sigma}$.

The diffusion coefficient obtained from continuum micromechanics according to Eq. (12), considering the effect of the micro-structure, can now be used to define the chemical potential, which can be written as

$$\Psi_c(\boldsymbol{\gamma}, \varphi_c^a, \phi_{chem}) = \frac{1}{2} \boldsymbol{\gamma} \cdot \mathbf{D}^c \cdot \boldsymbol{\gamma}, \quad (15)$$

where $\boldsymbol{\gamma} = -\nabla c$ and the resulting mass flux of ions is obtained as the derivative of the chemical potential Eq. (15), with respect to $\boldsymbol{\gamma}$.

$$\mathbf{J} = \frac{\partial \Psi_c}{\partial \boldsymbol{\gamma}} = -\mathbf{D}^c \cdot \nabla c. \quad (16)$$

3. MULTI-PHASE MODELING USING THE THEORY OF POROUS MEDIA: MODELING OF PHASE CHANGE IN FREEZING SOLIDS

The continuum mechanics description of porous materials as a multi-phase material whose behaviour is influenced by the interaction of the solid skeleton and the liquid and gaseous pore fluids can be accomplished either by using the micro-scale or macro-scale as a point of departure. The Theory of Mixtures [38] has been established as a suitable homogenization procedure, which allows to treat multi-phase materials as a continuum while each constituent may be described by its own kinematics and balance equations. The interactions between the constituents are considered by interaction terms within the balance equations. Since the Theory of Mixtures contains no microscopic information of the mixture, the enhancement by the concept of volume fractions is necessary, which leads to the well established concept of the Theory of Porous Media (TPM). It defines the volume fraction of each constituent dv_α and the volume of the mixture dv , which provides a representation of the local microscopic composition of multi-phase materials: $\phi_\alpha = dv_\alpha/dv$. The sum of the volume fractions of all constituents has to be equal to one: $\sum_\alpha \phi_\alpha = 1$.

3.1. Poromechanics of freezing processes

The modeling of the freezing process of the pore water contained in the pore structure of porous materials on a macroscopic scale requires consideration of coupled thermo-hydro-mechanical processes acting on various (lower) scales of the pore structure such as the multi-scale physics of confined crystallization of ice phase and the cryo-suction mechanism driving the liquid towards the frozen sites. For the macroscopic description of the mechanical behavior of water-infiltrated materials upon freezing the theory of poromechanics [7] provides a sound up-scaling framework and allows for a physics-oriented understanding. Within this framework the behavior of freezing porous materials is described, on the macroscopic scale, by the constitutive equations, the liquid-crystal equilibrium relation and liquid saturation curve in addition to the balance equations [41, 42].

Based upon the theory of unsaturated thermo-poro-elasticity proposed by Coussy [7], a three-phase finite-element model, consisting of solid particle (S), liquid water (L) and crystal ice (C), is present for the description of the freezing porous material. Consider an infinitesimal representative element extracted from such a porous continuum. In the reference configuration the volume of the element is $d\Omega_0$, and its porous volume is $\phi_0 d\Omega_0$, where ϕ_0 denotes the initial porosity. In the current configuration the porous volume is $\phi d\Omega_0$, ϕ denoting the current porosity. It is assumed, that the porous volume is completely filled by water, in both liquid form (index $J = L$) and crystal form (index $J = C$). The current LAGRANGIAN porosity ϕ can be written as

$$\phi = \phi_L + \phi_C, \quad \text{with} \quad \phi_J = \phi_0 S_J + \varphi_J, \quad (17)$$

where ϕ_J is the current LAGRANGIAN partial porosity related to phase J , φ_J is the respective change in partial porosity and S_J is the respective current saturation satisfying $S_L + S_C = 1$. The split of ϕ_J in Eq. (17) suggests that the change in the partial porosities ϕ_J results from two distinct processes: the invasion of the porous volume by ice crystal due to phase change, and the pressure action from the liquid and crystal phases to the internal walls of the skeleton.

3.1.1. Constitutive equations

The thermo-poroelastic constitutive equations can be derived using a thermodynamics-based approach proposed by Coussy [7]. For the same representative volume $d\Omega_0$ with an initial temperature T_0 and a (zero) reference pore pressure of atmospheric pressure, the total stress tensor $\boldsymbol{\sigma}$, the partial porosity change φ_J and the entropy of the solid matrix Σ_S are related to the strain tensor $\boldsymbol{\varepsilon}$, the pore pressures p_J and the temperature T via:

$$\sigma_{ij} = (K - 2G/3) \epsilon \delta_{ij} + 2G \varepsilon_{ij} - (b_L p_L + b_C p_C + 3aK(T - T_0)) \delta_{ij}, \quad (18)$$

$$\varphi_L = b_L \epsilon + \frac{p_L}{N_{LL}} + \frac{p_C}{N_{CL}} - a_L (T - T_0), \quad (19)$$

$$\varphi_C = b_C \epsilon + \frac{p_L}{N_{CL}} + \frac{p_C}{N_{CC}} - a_C (T - T_0), \quad (20)$$

$$\Sigma_S = \Sigma_{S0} + 3aK\epsilon - 3(a_L p_L + a_C p_C) + \frac{C_S}{T_0} (T - T_0). \quad (21)$$

In Eq. (18) $\epsilon = \varepsilon_{kk}$ is the volumetric dilation; K and G are respectively the effective bulk modulus and shear modulus; a , a_L and a_C are the thermal volumetric dilation coefficients related to the porous solid, liquid water and crystal ice, respectively; b_J and N_{JK} are the generalized BIOT coefficient and coupling moduli, while Σ_{S0} and C_S represent the volumetric initial entropy and heat capacity of the skeleton. The poroelastic properties involved in Eqs. (18)–(20) have to satisfy

compatibility [3]. Assuming that all pores deform the same when subjected to the same pore pressure, the macroscopic poroelastic properties are linked to the bulk modulus k_S and the thermal volumetric dilation coefficient α_S of the solid matrix according to the relations

$$b_J = b S_J, \quad b = 1 - \frac{K}{k_S}, \quad \frac{1}{N_{JJ}} + \frac{1}{N_{LC}} = \frac{b - \phi_0}{k_S} S_J, \quad (22)$$

$$a = \alpha_S, \quad a_J = \alpha_S (b - \phi_0) S_J,$$

where b is the BIOT coefficient related to the porous solid. For a micromechanics-oriented derivation of the poromechanics coupling coefficients for partially saturated porous materials, considering combined effects of plastic deformations and damage, we refer to [14, 25]. By adoption of the MORI-TANAKA homogenization scheme for a matrix-inclusion composite comprising a continuous matrix made of isotropic elastic solid and spherical voids [28], the bulk modulus K and the shear modulus G can be expressed in the form

$$K = \frac{4 k_S g_S (1 - \phi_0)}{3 \phi_0 k_S + 4 g_S}, \quad G = \frac{g_S (9 k_S + 8 g_S) (1 - \phi_0)}{6 \phi_0 (k_S + 2 g_S) + (9 k_S + 8 g_S)}. \quad (23)$$

Exploring the thermodynamic equilibrium between the liquid pore water (L) and the adjacent crystal ice (C) provides a relation between the crystal pressure p_C and liquid pressure p_L

$$p_C - p_L = \Sigma_f (T_f - T) \quad \text{with} \quad \Sigma_f = \frac{\rho_C L_f}{T_f}, \quad (24)$$

where T_f , Σ_f and L_f are the bulk freezing temperature, the freezing entropy and the latent heat of freezing, respectively. Equation (24) can be used to explain the cryo-suction process which has been identified as the driving force of the frost heave phenomenon [8]. At a temperature below the bulk freezing point, confined water can partially remain liquid provided that it de-pressurizes relative to the adjacent ice crystals, provoking, in turn, a cryo-pumping of the distant liquid water.

As a further ingredient of scale transition, the liquid saturation curve for a porous material saturated with liquid water and air (G) is inferred from the relation between the degree of liquid saturation and a macroscopic measure of interface forces acting between the pore water and the solid particles, generally denoted as the capillary pressure. Incorporating the VAN GENUCHTEN capillary function into the YOUNG-LAPLACE law at the gas-liquid interface provides a relationship between the liquid saturation and the pore size

$$S_L = \left(1 + \left(\frac{2 \gamma_{GL}}{\mathcal{N} R} \right)^{\frac{1}{1-m}} \right)^{-m} = F(R), \quad (25)$$

where γ_{GL} is the liquid-air interface energy, \mathcal{N} is a capillary modulus, R is the mean curvature radius of the interface and m is a constant representing the shape of the capillary curve. It implies that the remaining liquid saturation S_L equals the cumulative fraction $F(R)$ of pore volume occupied by pores having a pore entry smaller than R . Replacing the pore size R in Eq. (25) by the GIBBS-THOMSON law governing the liquid-crystal interface gives a relationship between the liquid saturation and the temperature

$$S_L = \left(1 + \left(\frac{T_f - T}{\Delta T_{ch}} \right)^{\frac{1}{1-m}} \right)^{-m}, \quad (26)$$

where ΔT_{ch} is the characteristic cooling temperature related to the most frequently encountered pore radius R_{ch} , and m is an index indicating the pore radius distribution around R_{ch} . Their influences on the shape of the saturation curve are illustrated in Fig. 5.

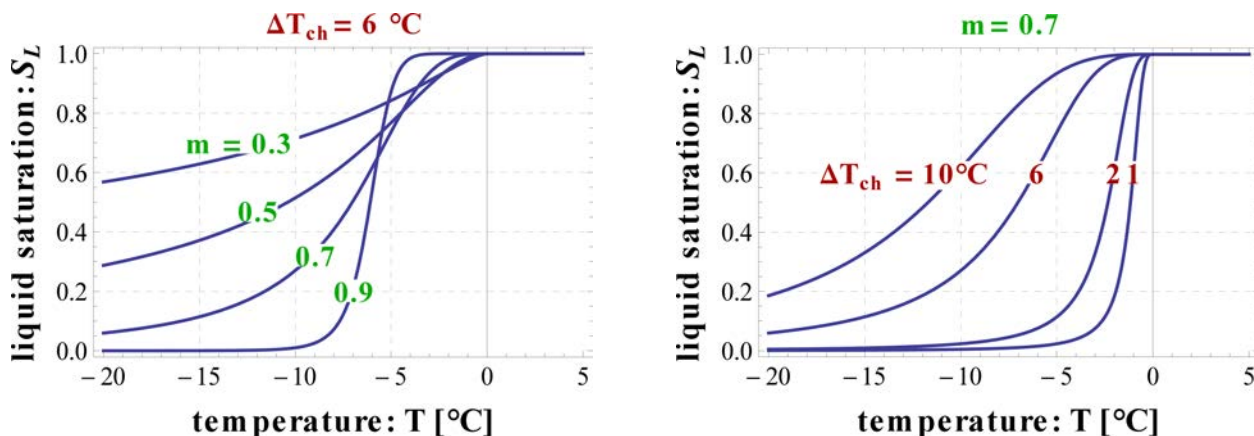


Fig. 5. Liquid saturation curve during freezing by influences of m (left) and ΔT_{ch} (right).

3.2. Thermo-hydro-mechanical finite element formulation

By choosing the solid displacement, the liquid water pressure and the mixture temperature as state variables, (1) mass balance of liquid water and crystal ice, (2) overall momentum balance and (3) overall entropy balance are set up as the governing set of balance equations. In the context of the finite element formulation of the model in a geometrically linear setting, the balance equations are transformed to their variational forms. For the spatial discretization of the initial boundary value problem, quadratic LAGRANGIAN shape functions are used for the approximation of the displacement field and linear shape functions are used for the approximations of the liquid pressure and the temperature. With such approximations the BABUSKA–BREZZI stability constraint is fulfilled [4]. For the temporal discretization, a modified midpoint rule, denoted as the generalized- α method is used, which ensures unconditional stability and second order accuracy for an appropriate choice of its parameters [20]. The discretized weak form, evaluated at the generalized midpoint, yields a highly nonlinear system of equations that is solved iteratively using NEWTON’s method. For the sake of simplicity, the tangent stiffness matrices required to solve the linearized system of algebraic equations are generated numerically according to the methodology presented by LEE & PARK [23]. Finally, the three-phase freezing model is implemented into the object-oriented FE-code KRATOS (DADVAND *et al.* [9]).

3.3. Model validation

The model performance with regards to the phase change behavior and the latent heat effect of freezing soils is investigated by comparing the numerical results with the phase-change model presented by LACKNER *et al.* [22], where only the thermal problem is considered. These model results represent validated results after comparison with results from experiments (for details we refer to [22]). A cuboidal, fully saturated sand specimen with a height of 0.09 m and a cross-section of $0.41 \times 0.41 \text{ m}^2$ with an initial temperature $T_i = 10^\circ\text{C}$ is considered. Three temperature sensors (A, B and C) are installed at different positions in the specimen, as shown in Fig. 6, for the monitoring of the temperature. At time $t = 0 \text{ s}$, the top surface is instantaneously subjected to freezing with a constant heat flux $q^* = -100 \text{ W/m}^2$; all the other surfaces are kept thermally isolated. The material properties involved in the validation test are listed in Table 2.

The obtained simulation results of the proposed model are compared with the validated numerical results in [22]. Both models indicate that, as soon as phase transition starts, the release of latent heat prevents the temperature from dropping. As long as the total released energy is consumed, a rapid temperature decrease is observed (Fig. 6 left). During the freezing process, the freezing front propagates through the specimen from the top to the bottom until the entire specimen is frozen

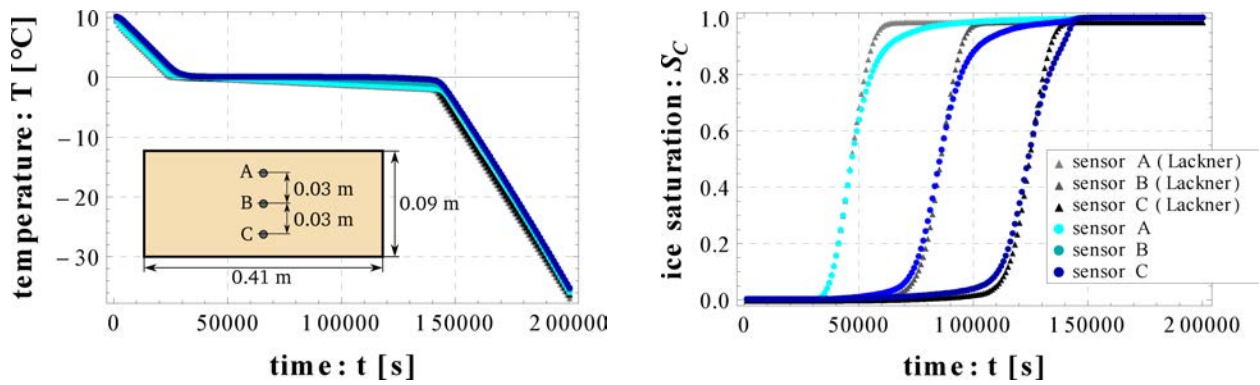


Fig. 6. Validation of model for freezing of porous materials: Temperature (left) and ice saturation (right) evolutions observed at the three sensor positions.

Table 2. Validation of model for freezing of porous materials: Material parameters.

Properties	Symbol	Numerical values	Units
Porosity	ϕ_0	0.42	
Bulk freezing temperature	T_f	273	K
Freezing entropy	Σ_f	1.2	MPa
Characteristic cooling	ΔT_{ch}	0.2	°C
Pore size distribution parameter	m	0.7	
Initial mass density	ρ_{S0}	2650	kg/m ³
	ρ_{L0}	1000	kg/m ³
	ρ_{C0}	913	Kg/m ³
Thermal conductivity	λ_S	7.694	W/(m K)
	λ_L	0.611	W/(m K)
	λ_C	2.222	W/(m K)
Heat capacity	c_S	740	J/(kg K)
	c_L	4200	J/(kg K)
	c_C	1900	J/(kg K)

(Fig. 6 right). The comparison shows a good correlation between the numerical model for both temperature and ice saturation evolutions. Only a slight difference appears in the ice saturation evolution curves (Fig. 6 right) due to the adoption of different liquid saturation functions.

4. FLUID FLOW IN CRACKS PROPAGATING IN POROUS MATERIALS: UP-SCALING FROM SINGLE CRACK TO STRUCTURAL LEVEL USING A TWO-PHASE EXTENDED FINITE ELEMENT METHOD

For the numerical analysis of undamaged porous materials, considering the transport of ions and liquid substances (water or moisture) through the pore space in addition to the mechanical loadings, the theory of poromechanics [6] as described in Sec. 3 is, by now, a well established approach. In computational structural analyses involving discontinuities such as evolving cracks in concrete structures, joints in rocks or shear bands in soft soils, however, the highly accelerated moisture transport in the opening discontinuities has to be taken into account. This again requires an appropriate up-scaling procedure from the spatial scale of the local crack, which usually is much smaller compared to the scale of typical finite elements used in structural analysis. In poromechanics problems, this scale transition refers to both the displacement field (discontinuity across cracks) as well

as to the fluid flow (accelerated flow within cracks and the communication with the flow within the bulk material).

Discontinuities such as cracks are characterized by a disturbance of the overall distribution of the field variables within a very small length. To resolve the small and the large scale portion of the solution, the Extended Finite Element method [27], exploiting the Partition of Unity property of shape functions, offers the possibility to include arbitrary enhancement functions into the finite element approximation to improve the local approximation of non-smooth distributions of field variables, such as discontinuities of the displacement field or the fluid pressure field across cracks [2, 15]. The Extended Finite Element Method is a variational multiscale method [16]. According to the variational multiscale method, the approximation spaces for the relevant field variables as well as for the associated test functions are decomposed into a coarse scale space $\overline{\mathcal{S}}$ and a fine scale space $\widehat{\mathcal{S}}$, which is associated with the fine scale resolution in the vicinity of cracks. The function spaces $\widehat{\mathcal{S}}$ are chosen according to the physical characteristics of the field variable at the fine scale, i.e., across the cracks.

4.1. Model description

Adopting poromechanics as the modeling framework, and assuming pores to be filled by an ideal mixture of water vapor and dry air, the two-field problem is characterized by the displacement field \mathbf{u} and the capillary pressure p_c as degrees of freedom. Accordingly, the variables that have to be locally enriched to better resolve the distribution in the vicinity of cracks, are the displacements \mathbf{u} and the capillary pressure p_c which are decomposed additively: $\mathbf{u} = \overline{\mathbf{u}} + \widehat{\mathbf{u}}$ and $p_c = \overline{p}_c + \widehat{p}_c$. Likewise, this additive split is applied to the respective test functions.

For an element fully crossed by a crack, the Sign function is used for the representation of the discontinuous displacement field across the crack.

$$\mathbf{u} = \overline{\mathbf{u}} + S_S \widehat{\mathbf{u}} \approx \sum_{i=1}^{n_r} N_i \overline{\mathbf{u}}_i^{nr} + S_S \sum_{i=1}^{n_c} N_i \widehat{\mathbf{u}}_i^{nc}, \quad (27)$$

where n_r is the number of nodes used for the spatial discretization of the regular displacement field (superscript r). In coupled hygro-mechanical problems involving porous materials with cracks, the flow of the pore fluid across the crack will be discontinuous (Fig. 7). Considering a jump of the moisture flux across the discontinuity $\partial_S \Omega$ leads to the weak form of the mass balance (for details, we refer to [24, 30]),

$$\int_{\Omega} \delta p_c \frac{\dot{m}_l}{\rho_l} dV - \int_{\Omega} \delta \nabla p_c \cdot \mathbf{q}_l dV + \int_{\partial_S \Omega} \delta p_c [\mathbf{q}_l] \cdot \mathbf{n}_S dA = \int_{\Gamma_q} \delta p_c q_l^* dA. \quad (28)$$

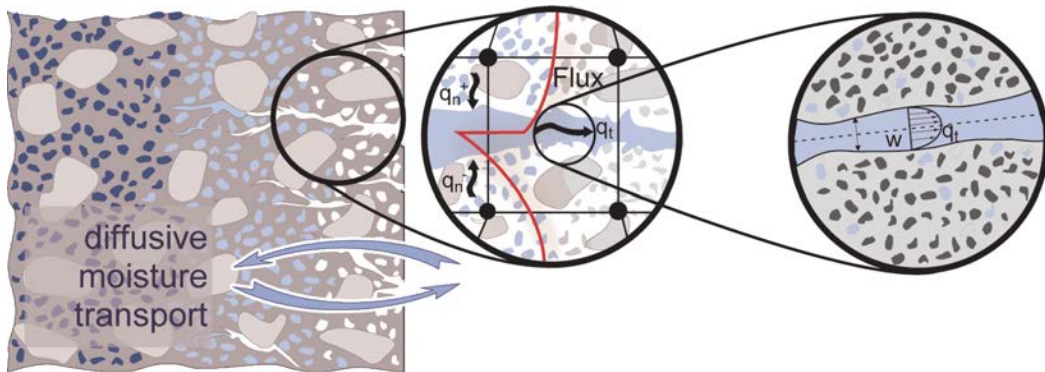


Fig. 7. Transport in porous materials across cracks as a multiscale problem.

For the fluid flow \mathbf{q}_l in the porous medium, Darcy's relation is used:

$$\mathbf{q}_l = \frac{\mathbf{k}}{\mu_l} \cdot \nabla p_c. \quad (29)$$

\mathbf{k} denotes the macroscopic permeability tensor and μ_l the dynamic viscosity of the fluid. The opening of discontinuities leads to an increase of the permeability at the discontinuity. This effect can be simulated by splitting the macroscopic permeability tensor \mathbf{k} into a part associated with the bulk material \mathbf{k}_f and in a part associated with the crack k_c^t [33]. Darcy's relation for the bulk material yields

$$\mathbf{q}_l = \frac{\mathbf{k}_f}{\mu_l} \nabla p_c. \quad (30)$$

In Eq. (30), the permeability \mathbf{k}_f of the uncracked porous medium:

$$\mathbf{k}_f(S_l, \phi) = k_r(S_l) k_\phi(\phi) \mathbf{k}_0 \quad (31)$$

depends on the relative permeability factor $k_r(S_l)$ for water [39]

$$k_r(S_l) = \sqrt{S_l} \left[1 - (1 - S_l^{1/m})^m \right]^2 \quad \text{with} \quad 0 < m < 1, \quad (32)$$

on the permeability factor $k_\phi(\phi)$ related to the porosity of the porous medium

$$k_\phi(\phi) = 10^\delta \quad \text{with} \quad \delta = \frac{6(\phi - \phi_0)}{0.3 - 0.4\phi_0} \quad (33)$$

and on the intrinsic permeability of the fully saturated, uncracked medium \mathbf{k}_0 . In this contribution the porosity is assumed to be constant throughout the numerical simulation ($\phi = \phi_0$). Based on the solution of the *Navier-Stokes* equation, a parabolic velocity profile across the cavity is assumed (see Fig. 7). Hence, the fluid flow in tangential direction at the discontinuity yields

$$q_l^t = \frac{w_c^2}{12\mu_l} \nabla^t p_c. \quad (34)$$

With this assumption, a crack permeability k_c^t as a function of the hydraulic crack width $w = w_h$ can be identified. The hydraulic crack width

$$w_h = \frac{w_c^2}{R^{2.5}} \quad \text{for} \quad w_c \geq w_h \quad (35)$$

describes the distance of parallel faces of the cavity and depends on the roughness R of the material [1], e.g., $R = 15$ for concrete. The crack dependent permeability k_c^t is defined as follows:

$$k_c^t(S_l, w) = k_{rc}(S_l) k_{c,0}^t(w), \quad (36)$$

where k_{rc} denotes the relative permeability factor for water in the cavity

$$k_{rc}(S_l) = 8 \cdot 10^{-6} \exp(11.7 \cdot S_l) \quad (37)$$

and $k_{c,0}^t(w)$ denotes the dependency of the crack width on the permeability in tangential direction of the crack

$$k_{c,0}^t(w_h) = \frac{w_h^2}{12}. \quad (38)$$

Integration across the crack width and considering the local mass balance at the discontinuity (i.e., on the small scale level) provides the expression appearing in Eq. (28) for the normal component of the moisture flux across the crack related to the fluid mass transport in the tangential direction of the crack.

The capillary pressure is discretized using a local enhanced partition of unity approximation of the local C^1 discontinuity of the pressure across the crack:

$$p_c = \bar{p}_c + \hat{p}_c \approx \sum_{i=1}^{NN} N_i \bar{p}_c^{ei} + \sum_{j=1}^{NE} \underbrace{N_j \psi^j}_{N_j^{enr}} \hat{p}_c^e = \mathbf{N}_{\bar{p}} \bar{\mathbf{p}}_c^e + \mathbf{N}_{\hat{p}}^{enr} \hat{\mathbf{p}}_c^e. \quad (39)$$

In Eq. (39) the function ψ is related to the distance function. Figure 8 illustrates the functions used for the enhanced approximations of the displacement field \mathbf{u} and the capillary pressure p_c .

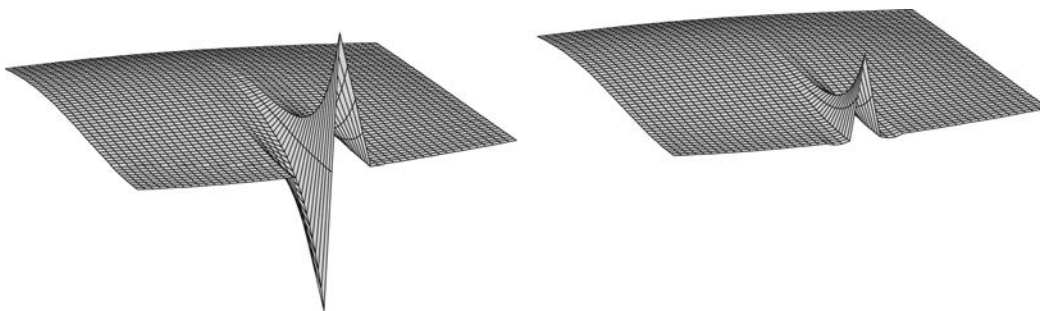


Fig. 8. Enhanced approximations of displacements (left) and capillary pressure (right).

4.2. Model validation

For the validation of the two-phase X-FEM model, numerical results were compared with experimental results published in [31], where the water uptake in fractured brick samples with different crack widths was measured using X-ray radiography. After the brick samples were dried out (105°C) the specimens were placed on water and the water uptake was measured in regular time intervals. Table 3 contains the material properties for this validation example. After prescribing an initial capillary pressure $p_c^{\text{ini}} = 10$ MPa in the complete domain, which is correlated to a saturation of $S(p_c) = 0.013$, the capillary pressure at the bases of the brick samples was decreased to $p_c = 0.00001$ MPa ($S(p_c) = 1$) in several time steps to avoid numerical oscillations. The mesh of the brick sample consists of 900 quadrilateral elements using bi-quadratic shape functions for the approximations of the displacement and the capillary pressure field. The distributions of the saturation in the brick samples for two different crack widths, $w = 0.1$ mm and $w = 0.01$ mm are

Table 3. Material parameters.

Properties	Symbol	Value
Young's modulus	E	16700 MPa
Poisson's ratio	ν	0
Initial porosity	ϕ_0	0.157
Biot coefficient	b	0.7
Intrinsic permeability	k_0	$1.906 \cdot 10^{-15} \text{ m}^2$
Dyn. viscosity (water)	μ_l	$1 \cdot 10^{-9} \text{ MPa s}$
Reference pressure	p_r	18.6 MPa
Porosity index	m	0.7

illustrated in Fig. 9a and 9b. In Fig. 9c the experimental results are compared to the numerical results. Here, the advancement of the saturation front is plotted over time for both investigated crack widths. The agreement is in both cases excellent. From this comparison it can be concluded that the accelerated moisture transport in cracked cementitious materials can be well represented by the proposed two-phase X-FEM model.

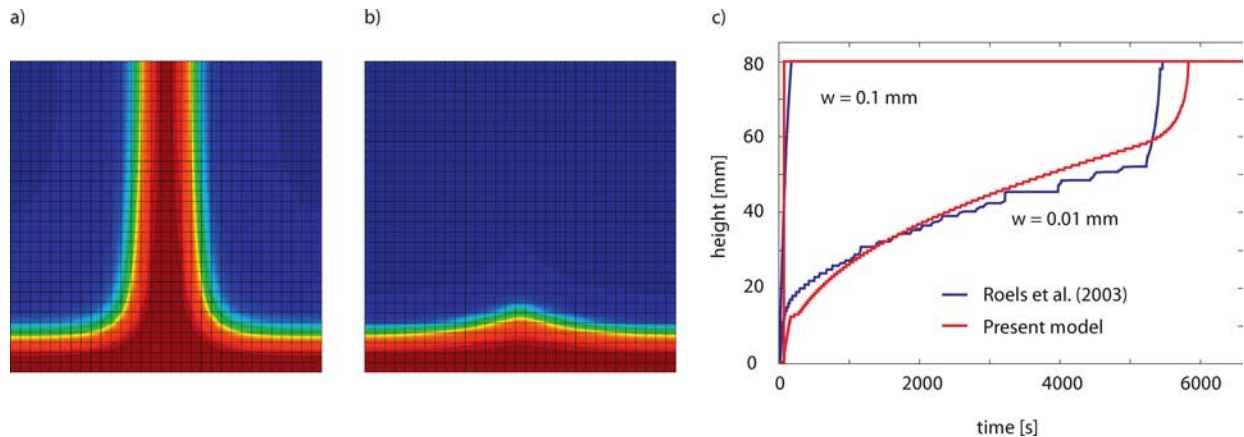


Fig. 9. a) Distribution of the saturation at $t = 150$ s ($w = 0.1$ mm); b) distribution of the saturation at $t = 600$ s ($w = 0.01$ mm); c) evolution of the saturation front in time: Experimental vs. numerical results.

5. CONCLUDING REMARKS

The paper has provided a synthesis of scale-bridging modeling and discretization strategies for multiphase materials. A micromechanics model was proposed to obtain macroscopic transport properties. This allows to incorporate essential topological information from the nano- to the meso-level into a macroscopic model using, e.g., poromechanics. The theory of poromechanics, using a three-field formulation, provided the modeling framework at the macroscopic level to describe phenomena acting at lower scales such as the crystallization of the ice phase and the cryo-suction mechanism involved in freezing processes of porous materials. For the up-scaling of local disturbances of the displacement field and the fluid flow when cracks open and propagate in porous materials, a two-field Extended Finite Element method, formulated in the framework of poromechanics, was proposed as a variational multiscale type method to represent the distribution of the field variables in the vicinity of cracks at the spatial scale of finite elements. It was shown, that this model adequately describes the coupled hygro-mechanical processes in cracked porous materials. Exploiting the potentials of each sub-model opens the perspective to further increase the ability of computational simulations of structures made of multiphase materials to capture the essential physical mechanisms and to reduce the phenomenological character of the underlying models.

REFERENCES

- [1] N. Barton, S. Bandis, and K. Bakhtar. Strength, deformation and conductivity coupling of rock joints. *International Journal of Rock Mechanics and Mining Sciences & Geomechanics Abstracts*, **22**: 121–140, 1985.
- [2] C. Becker, S. Jox, and G. Meschke. 3D higher-order X-FEM model for the simulation of cohesive cracks in cementitious materials considering hygro-mechanical couplings. *Computer Modeling in Engineering and Sciences*, **57**(3): 245–276, 2010.
- [3] M.A. Biot. General theory of three-dimensional consolidation. *Journal of Applied Physics*, **12**: 155–165, 1941.
- [4] F. Brezzi and M. Fortin. *Mixed and Hybrid Finite Element Methods*. Springer, Berlin, 1991.
- [5] M. Cieszko. Description of anisotropic pore space structure of permeable materials based on Minkowski metric space. *Arch. Mech.*, **61**: 425–444, 2009.
- [6] O. Coussy. *Mechanics of Porous Continua*. John Wiley & Sons, Chichester, 1995.
- [7] O. Coussy. Poromechanics of freezing materials. *J. Mech. Phys. Solids*, **53**: 1389–1718, 2005.

- [8] O. Coussy and P. Monteiro. Poroelastic model for concrete exposed to freezing temperatures. *Cement and Concrete Research*, **38**: 40–48, 2008.
- [9] P. Dadvand, J. Mora, C. González, A. Arraez, P.A. Ubach, and E. Oñate. KRATOS: An Object-Oriented Environment for Development of Multi-Physics Analysis Software. In H.A. Mang, F.G. Rammerstorfer, and J. Eberhardsteiner, editors, *WCCM V, Fifth World Congress on Computational Mechanics*, 2002.
- [10] A. Delagrave, B. Gérard, and J. Marchand. Modelling the calcium leaching mechanisms in hydrated cement pastes. In K.L. Scrivener and J.F. Young, editors, *Mechanisms of Chemical Degradation of Cement-based Systems*, pages 38–49, London, 1997. Chapman & Hall.
- [11] L. Dormieux and E. Lemarchand. Homogenization approach of advection and diffusion in cracked porous material. *American Society of Civil Engineers - Engineering Mechanics*, **127**(12): 1267–1274, 2001.
- [12] J.D. Eshelby. The determination of the elastic field of an ellipsoidal inclusion, and related problems. *Proc. R. Soc. Lond. A*, **241**: 376–396, 1957.
- [13] B. Gérard. *Contribution des Couplages Mécanique-Chimie-Transfert dans la Tenue a long Terme des Ouvrages de Stockage de Déchets Radioactifs*. Ph.D. Thesis, Laboratoire de Mécanique et Technologie. E.N.S. de Cachan, 1996.
- [14] S. Grasberger and G. Meschke. Thermo-hygro-mechanical degradation of concrete: From coupled 3D material modelling to durability-oriented multifield structural analyses. *Materials and Structures*, **37**: 244–256, May 2004. Special Issue on Poromechanis of Concrete.
- [15] G. Hofstetter and G. Meschke, editors. *Numerical Modeling of Concrete Cracking*, volume 532 of *CISM Courses and Lectures*. Springer Wien New York, 2011. 327 pages.
- [16] T.J.R. Hughes, G.R. Feijóo, L. Mazzei, and J.B. Quincy. The variational multiscale method: a paradigm for computational mechanics. *Computer Methods in Applied Mechanics and Engineering*, 166:3–24, 1998.
- [17] V. Kouznetsova, M.G.D. Geers, and W.A.M. Brekelmans. Multi-scale constitutive modelling of heterogeneous materials with a gradient-enhanced computational homogenization scheme. *International Journal for Numerical Methods in Engineering*, **54**: 1235–1260, 2002.
- [18] J. Kuschwitz, I. Bevanda, S. Krimpmann, D. Kuhl, M. Setzer, and G. Meschke. Durability of cementitious materials and the role of the pore structure: Experimental observations and numerical modelling. In F. Stangenberg, O.T. Bruhns, D. Hartmann, and G. Meschke, editors, *Life-time oriented Design Concepts*, pages 449–470. SFB 398, 2007.
- [19] D. Kuhl, F. Bangert, and G. Meschke. Coupled chemo-mechanical deterioration of cementitious materials. Part 1: Modeling. *International Journal for Solids and Structures*, **41**: 15–40, 2004.
- [20] D. Kuhl and M.A. Crisfield. Energy-conserving and decaying algorithms in non-linear structural dynamics. *Int. J. Num. Meth. in Eng.*, **45**(5): 569–599, 1999.
- [21] D. Kuhl and G. Meschke. Computational modeling of transport mechanisms in reactive porous media – application to calcium leaching of concrete. In R. de Borst, H.A. Mang, N. Bićanić, and G. Meschke, editors, *Computational Modelling of Concrete Structures*, pp. 473–482. Balkema, 2003.
- [22] R. Lackner, A. Amon, and H. Lager. Artificial ground freezing of fully saturated soil: Thermal problem. *Journal of Engineering Mechanics*, **131**(2): 211–220, February 2005.
- [23] Y. Lee and K.C. Park. Numerically generated tangent stiffness matrices for nonlinear structural analysis. *Computer Methods in Applied Mechanics and Engineering*, **191**(51–52): 5833–5846, 2002.
- [24] D. Leonhart and G. Meschke. Extended finite element method for hygro-mechanical analysis of crack propagation in porous materials. *Proceedings in Applied Mathematics and Mechanics*, 2011, DOI: 10.1002/pamm.201110072.
- [25] G. Meschke and S. Grasberger. Numerical modelling of coupled hygro-mechanical degradation of cementitious materials. *American Society of Civil Engineers - Engineering Mechanics*, **129**(4): 383–392, 2003.
- [26] C. Miehe and C. G. Bayreuther. On multiscale FE analyses of heterogeneous structures: From homogenization to multigrid solvers. *International Journal for Numerical Methods in Engineering*, **71**: 1135–1180, 2007.
- [27] N. Moës, J.E. Dolbow, and T. Belytschko. A finite element method for crack growth without remeshing. *International Journal for Numerical Methods in Engineering*, **46**: 131–150, 1999.
- [28] T. Mori and K. Tanaka. Average stress in the matrix and average elastic energy of materials with misfitting inclusions. *Acta Metallica*, **21**(5): 571–574, 1973.
- [29] L. Onsager and R. M. Fuoss. Irreversible processes in electrolytes. Diffusion, conductance, and viscous flow in arbitrary mixtures of strong electrolytes. *Journal of Physical Chemistry*, **36**: 2689–2778, 1932.
- [30] J. Rethore, R. de Borst, and M.-A. Abellan. A two-scale model for fluid in an unsaturated porous medium with cohesive cracks. *Computational Mechanics*, **42**: 227–238, 2008.
- [31] S. Roels, K. Vandersteen, and J. Carmeliet. Measuring and simulating moisture uptake in a fractured porous medium. *Advances in Water Resources*, **26**: 237–246, 2003.
- [32] L. Shen and Z. Chen. Critical review of the impact of tortuosity on diffusion. *Chemical Engineering Science*, **62**: 3748–3755, 2007.
- [33] D.T. Snow. Anisotropic permeability of fractured media. *Water Resources Research*, **5**: 1273–1289, 1969.
- [34] F. Stangenberg, R. Breitenbücher, O.T. Bruhns, D. Hartmann, D. Kuhl, and G. Meschke, editors. *Lifetime-Oriented Structural Design Concepts*. Springer Berlin, 2009.

-
- [35] J. J. Timothy and G. Meschke. A cascade micromechanics model for diffusion in porous materials. *J. Mech. Phys. Solids*, submitted for publication, 2011.
- [36] J. J. Timothy and G. Meschke. Micromechanics model for tortuosity and homogenized diffusion properties of porous materials with distributed micro-cracks. *Proceedings in Applied Mathematics and Mechanics*, 2011, DOI: 10.1002/pamm.201110267.
- [37] J. J. Timothy and G. Meschke. Cascade micromechanics model for diffusion in micro-cracked porous materials. *Cement & Concrete Research*, 2012, in preparation.
- [38] C. Truesdell. The rational mechanics of materials. In *On the foundations of Mechanics and Energetics*, pp. 293–304. Gordon & Breach, New York, 1965.
- [39] M.T. van Genuchten. A closed-form equation for predicting the hydraulic conductivity of unsaturated soils. *Soil Science Society of America*, 44:892–898, 1980.
- [40] A. Zaoui. Continuum micromechanics: Survey. *Journal of Engineering Mechanics*, **128**(8): 808–816, 2002.
- [41] M. Zhou and G. Meschke. Numerical modelling of coupling mechanisms during freezing in porous materials. In *Proceedings in Applied Mathematics and Mechanics*, 2011, DOI: 10.1002/pamm.201110239.
- [42] M. Zhou and G. Meschke. A three-phase finite element model of water-infiltrated porous materials subjected to freezing. In M. Papadarakakis, E. Onate, and B. Schrefler, editors, *Coupled Problems 2011*. CIMNE, 2011. CD-Rom, ISBN: 978-84-87867-59-0.